Geochemistry Geophysics Geosystems G3

Article
Volume 12, Number 9
10 September 2011
Q0AB10, doi:10.1029/2011GC003662
ISSN: 1525-2027

Published by AGU and the Geochemical Society

Pulses of deformation reveal frequently recurring shallow magmatic activity beneath the Main Ethiopian Rift

J. Biggs and I. D. Bastow
Department of Earth Sciences, University of Bristol, Wills Memorial Building, Queen's Street, Bristol BS8 1RJ, UK (juliet.biggs@bristol.ac.uk)

D. Keir
National Oceanography Centre, Southampton SO14 3ZH, UK

E. Lewi
IGSSA, Addis Ababa University, PO Box 1176, Addis Ababa, Ethiopia

[1] Magmatism strongly influences continental rift development, yet the mechanism, distribution, and timescales on which melt is emplaced and erupted through the shallow crust are not well characterized. The Main Ethiopian Rift (MER) has experienced significant volcanism, and the mantle beneath is characterized by high temperatures and partial melt. Despite its magma-rich geological record, only one eruption has been historically recorded, and no dedicated monitoring networks exist. Consequently, the present-day magmatic processes in the region remain poorly documented, and the associated hazards are neglected. We use satellite-based interferometric synthetic aperture radar observations to demonstrate that significant deformation has occurring at four volcanic edifices in the MER (Alutu, Corbetti, Bora, and Haledebi) from 1993 to 2010. This raises the number of volcanoes known to be deforming in East Africa beyond 12, comparable to many subduction arcs despite the smaller number of recorded eruptions. The largest displacements are at Alutu volcano, the site of a geothermal plant, which showed two pulses of rapid inflation (10–15 cm) in 2004 and 2008 separated by gradual subsidence. Our observations indicate a shallow (<10 km), frequently replenished zone of magma storage associated with volcanic edifices and add to the growing body of observations that indicate shallow magmatic processes operating on a decadal timescale are ubiquitous throughout the East African Rift. In the absence of detailed historical records of volcanic activity, satellite-based observations of monitoring parameters, such as deformation, could play an important role in assessing volcanic hazard.

Components: 6400 words, 6 figures, 2 tables.

Keywords: InSAR; continental rifting; magmatic processes; volcano deformation.

Index Terms: 1240 Geodesy and Gravity: Satellite geodesy: results (6929, 7215, 7230, 7240); 8105 Tectonophysics: Continental margins: divergent (1212, 8124); 8485 Volcanology: Remote sensing of volcanoes (4337).

Received 15 April 2011; **Revised** 15 June 2011; **Accepted** 15 June 2011; **Published** 10 September 2011.

Biggs, J., I. D. Bastow, D. Keir, and E. Lewi (2011), Pulses of deformation reveal frequently recurring shallow magmatic activity beneath the Main Ethiopian Rift, *Geochem. Geophys. Geosyst.*, *12*, Q0AB10, doi:10.1029/2011GC003662.

Theme: Magma-Rich Extensional Regimes
Guest Editors: R. Meyer, J. van Wijk, A. Breivik, and C. Tegner

1. Introduction

[2] As a continental rift develops towards a new oceanic spreading center, extension initially accommodated in a broad zone of faulting and ductile stretching transitions towards a narrower zone of focused magmatic intrusion [e.g., *Ebinger and Casey*, 2001]. The spatial and temporal variations in strain partitioning between faulting and magmatism during progressive extension plays a vital role in determining the continental rheology as well as local volcanic and seismic hazard.

[3] Recent geophysical and geochemical experiments in the Main Ethiopian Rift (MER) highlight the importance of magmatism in achieving extension during continental breakup [e.g., *Keranen et al.*, 2004; *Mackenzie et al.*, 2005; *Bastow et al.*, 2011]. The 60 km wide rift valley is bound by steep, large offset, border faults that accommodated extension during the Miocene [*Woldegabriel et al.*, 1990; *Wolfenden et al.*, 2004]. Since the Quaternary, strain has localized to discrete, ~20 km wide zones of volcanism and small offset faulting where extension occurs predominantly through magma intrusion with little crustal thinning [e.g., *Ebinger and Casey*, 2001; *Mackenzie et al.*, 2005; *Maguire et al.*, 2006]. This narrow zone of localized strain in Quaternary magmatic segments is often termed the Wonji Fault Belt (WFB). Petrographic modeling, thermodynamic modeling and single clinopyroxene pressure estimates have shown that the magmas predominantly fractionate in the upper crust [*Rooney et al.*, 2011]. Rhyolitic magmatism is associated with regularly spaced (20–50 km) central volcanoes of diameter >10 km, while basalts are usually associated with monogenetic vents or fissure eruptions along magmatic segments [*Mazzarini and Isola*, 2010] (Figure 1).

[4] Between 8 and 9.5°N, the along-rift peak in volume of Quaternary-Recent volcanism [*Abebe et al.*, 2007] coincides with a peak in seismic anisotropy of the lithosphere and low seismic velocities in the mantle [*Bastow et al.*, 2010; *Kendall et al.*, 2006]. Together, these observations suggest that the greatest melt supply, likelihood of volcanic eruption and geothermal potential lies between Gedemsa and Dofen volcanoes (Figure 1). South of 8°N, geophysical constraints are sparse nonetheless the distribution of seismicity [*Keir et al.*, 2009], Moho topography [*Tiberi et al.*, 2005], combined with geological observations [*Ebinger et al.*, 2000] suggest the deformation is more diffuse, with melt intrusion expected to play a lesser role in accommodating extension [*Ebinger and Hayward*, 1996].

[5] Despite the numerous studies concerning the behavior and significance of magmatism on geological timescales, little is known regarding the short-term activity of these volcanoes. Eruptions are believed to have occurred in the 1800s at Fentale and Kone [*Rampey et al.*, 2010] and many others are quotes as having undated lava flows with youthful-looking morphology [*Siebert and Simkin*, 2002]. The World Bank report on volcanic hazard lists all these volcanoes at a zero level of monitoring and the highest level of uncertainty in terms of hazard and risk [*Aspinall et al.*, 2011].

[6] Here we present interferometric synthetic aperture radar (InSAR) observations from the seismically active MER (Figure 1), which encompasses the transition between mechanical and magmatic extension during the breakup of a continent [e.g., *Ebinger and Casey*, 2001; *Wolfenden et al.*, 2004]. We investigate the spatial and temporal characteristics of deformation and explore its source location, depth and geometry before placing the observations in the context of global volcanism, rift development, geohazard and geothermal potential.

2. Geodetic Observations and Modeling

2.1. Satellite Radar Archive

[7] InSAR provides a powerful tool to measure surface deformation associated with tectonic and magmatic processes across plate boundary zones. The temporal and spatial characteristics of the deformation patterns allow us to discriminate between dike intrusion, faulting and magma chamber pressure changes [e.g., *Wright et al.*, 2006; *Pritchard and Simons*, 2004; *Massonnet et al.*, 1993].

[8] Studies of surface deformation are frequently motivated by observations of seismic or eruptive activity, in which case the location and timing of the event are already known. However, in this case, no external information exists to guide our observations and we perform a systematic search of all available satellite radar data, extending back to 1993. The Envisat background mission (2003–2010) acquired three to four images per year over the MER. Before this, the archive is more limited: ERS1/2 collected images in 1993, 1997, 2000 and a few images are available form the Japanese Space Agency satellite JERS between 1994 and 1996.

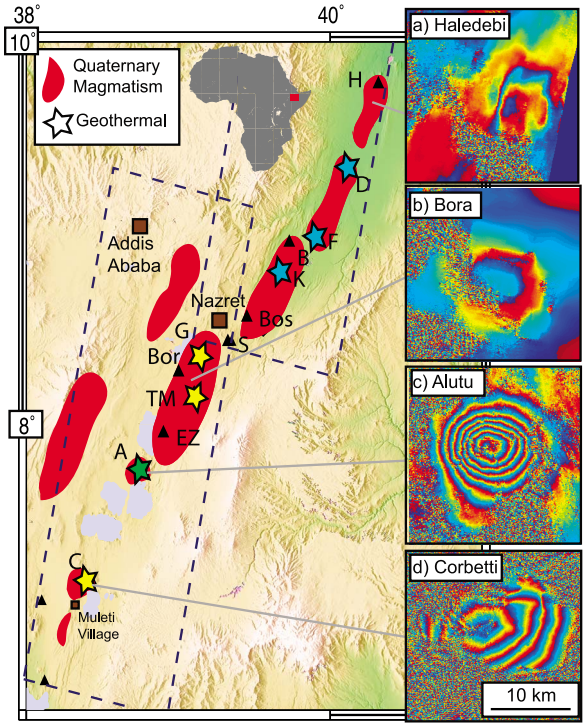

Figure 1. Main Ethiopian Rift. Insets show example interferograms for (a) uplift at Haledebi (24 August 2007 to 11 November 2007), (b) uplift at Bora (27 August 2008 to 23 June 2010), (c) uplift at Alutu (17 December 2003 to 18 August 2004), and (d) subsidence at Corbetti (23 September 1997 to 13 September 2000). Each fringe represents 2.8 cm of motion in the satellite line-of-sight. Volcanoes from the Smithsonian Database are denoted with black triangles or colored stars: green stars denote production plants, blue stars denote detailed exploration, and yellow stars denote prefeasibility studies. H, Hertali; D, Dofen; F, Fentale; B, Beru; K, Kone; B, Boset; S, Sodore; G, Gedemsa; Bor, Bora Berricio; TM, Tulla Moje; EZ, East Ziway; A, Alutu; C, Corbetti. Squares mark the major cities of Addis Ababa, Nazret, and Awasa. Lakes are marked in pale blue. Dashed rectangles are the coverage of Envisat Image Mode data from two tracks.

[9] Initially we produce annual interferograms (Figures 2 and 3) to identify areas of particular interest. We use the JPL software ROI_PAC and a 90 m SRTM DEM. For each, we process and unwrap all available interferometric pairs and construct a time series of deformation using a minimum norm velocity constraint [e.g., *Berardino et al.*, 2002; *Biggs et al.*, 2010]. Errors on each time step are estimated assuming a 1 cm error on each interferogram (Figure 3); the cumulative error of <4 cm is dominated by the early time steps [*Biggs et al.*, 2010].

2.2. Sources of Deformation

[10] We identify four areas of significant deformation: (1) Alutu volcano; (2) Corbetti volcano; (3) the area between Bora Berrichio and Tulla Moje volcano (hereafter referred to as Bora), and (4) Haledebi volcano in the Angelele segment (Figure 4). At Alutu (1) and Corbetti (2) the circular deformation pattern is centered on the volcano (Figures 1c and 1d). Similar circular deformation at Bora (3) is located in a low-lying area between the edifices of Bora Berrichio and Tulla Moje (Figure 1b). At Corbetti, four to five fringes of subsidence appear in two independent interferograms (ascending and descending tracks) over 1997–2000. Deformation extends beyond the patch of coherence associated with the edifice so the estimated displacement (14 cm) is a minimum. The JERS interferogram from 1994 to 1996 shows a small amount of uplift (1.4 cm) centered on the volcano but is dominated by a long-wavelength ramp due to a lack of orbital information.

[11] The northernmost signal, Haledebi, is located within the Angelele volcanic segment, >10 km south of Hertali volcano. Although the deformation is not associated with a catalogued volcano, a large volcanic edifice, with fresh-looking lava flows, is clearly visible in optical satellite images and digital elevation models. The deformation pattern is strongly asymmetric with a sharp boundary on the western side aligned with the local NNE-SSW rift trend suggesting a structural control (Figure 1a).

2.3. Source Models

[12] To estimate the dimensions and location of each source (Figure 5 and Table 1) we use a nonlinear inversion to find the optimum parameters for a range of analytic solutions: a point source [*Mogi*, 1958], a uniform pressure, a penny-shaped crack [*Fialko et al.*, 2001] and a rectangular dislocation [*Okada*, 1985].

[13] The best fitting source model for the deformation patterns at Alutu and Bora (Figure 6) is a shallow (<2.5 km) penny-shaped crack with large radius (3–10 km), similar to the best-fitting models for deformation at the Kenyan volcanoes [*Biggs et al.*, 2009b]. While a deeper point source also produces a radially symmetric deformation pattern, the predicted line-of-sight displacements are asymmetric due to the horizontal displacement component. Thus, a shallower penny-shaped model, which has larger ratio of vertical to horizontal displacement, produces a more symmetric line-of-sight displace-

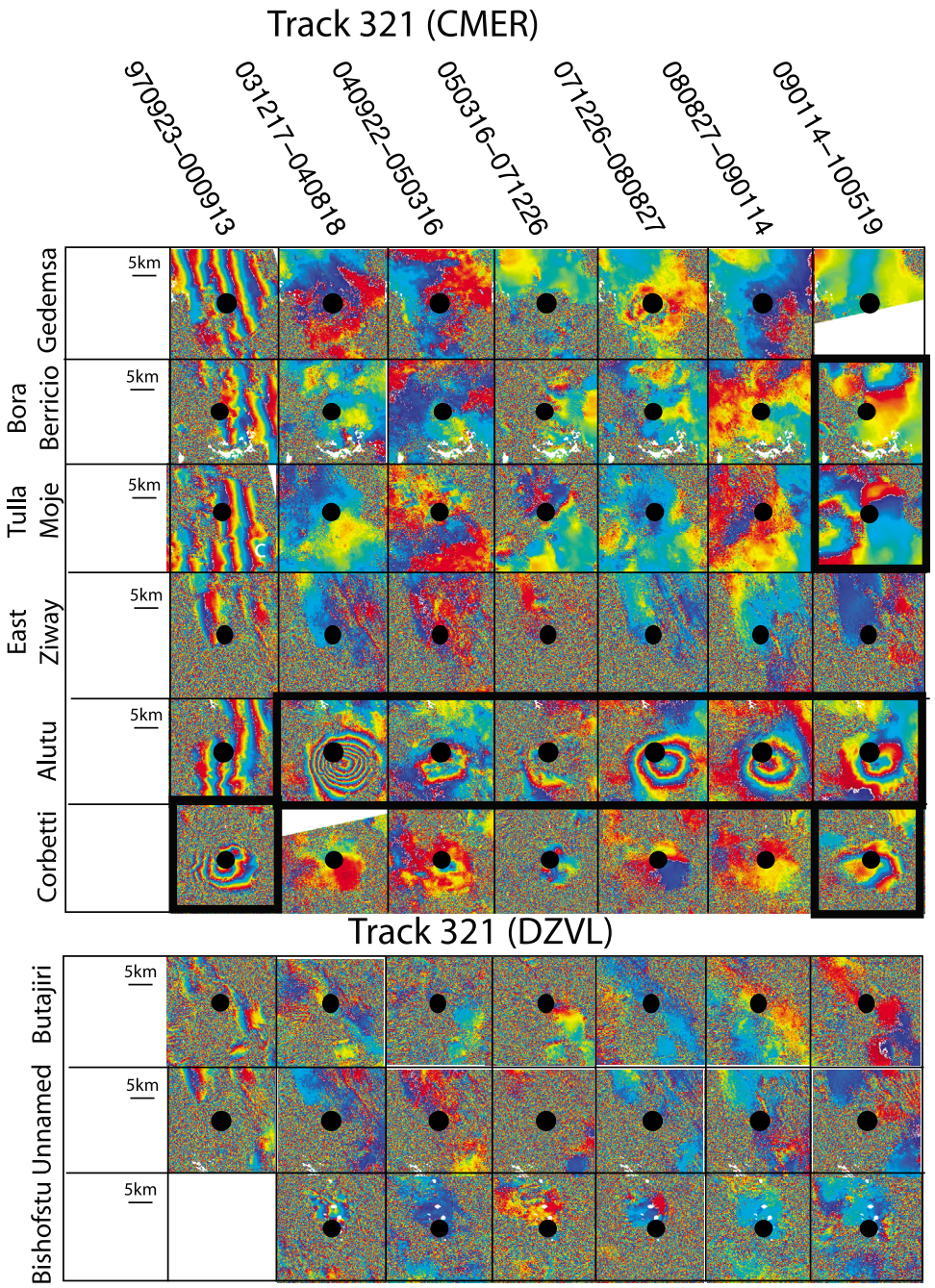

Figure 2. Survey interferograms from JERS, ERS, and Envisat for the central MER. Each color cycle (fringe) represents 2.8 cm of displacement in the satellite line-of-sight. The black dot is the summit, according to the Smithsonian Database [*Siebert and Simkin*, 2002]. Black rectangles highlight interferograms in which deformation is visible.

ment pattern and always results in a lower root-mean-square misfit. The deformation at Corbetti is better fit by a deeper (~5 km) point source, but this may be due to the coherence-limited coverage.

[14] The asymmetry in the deformation pattern at Haledebi indicates a significantly different geometry to the other sites, and specifically, that structural features, such as faults, may influence the deformation. The temporal characteristics of the deformation, specifically that the direction of motion reverses, makes it unlikely that the deformation can be explained by fault creep. Furthermore, the reversal of sign does not follow an annual pattern ruling out aquifer drainage and recharge. The pattern can be fit by a sill dipping at 10–20°W at a depth of 2.7–8.8 km (Figure 5).

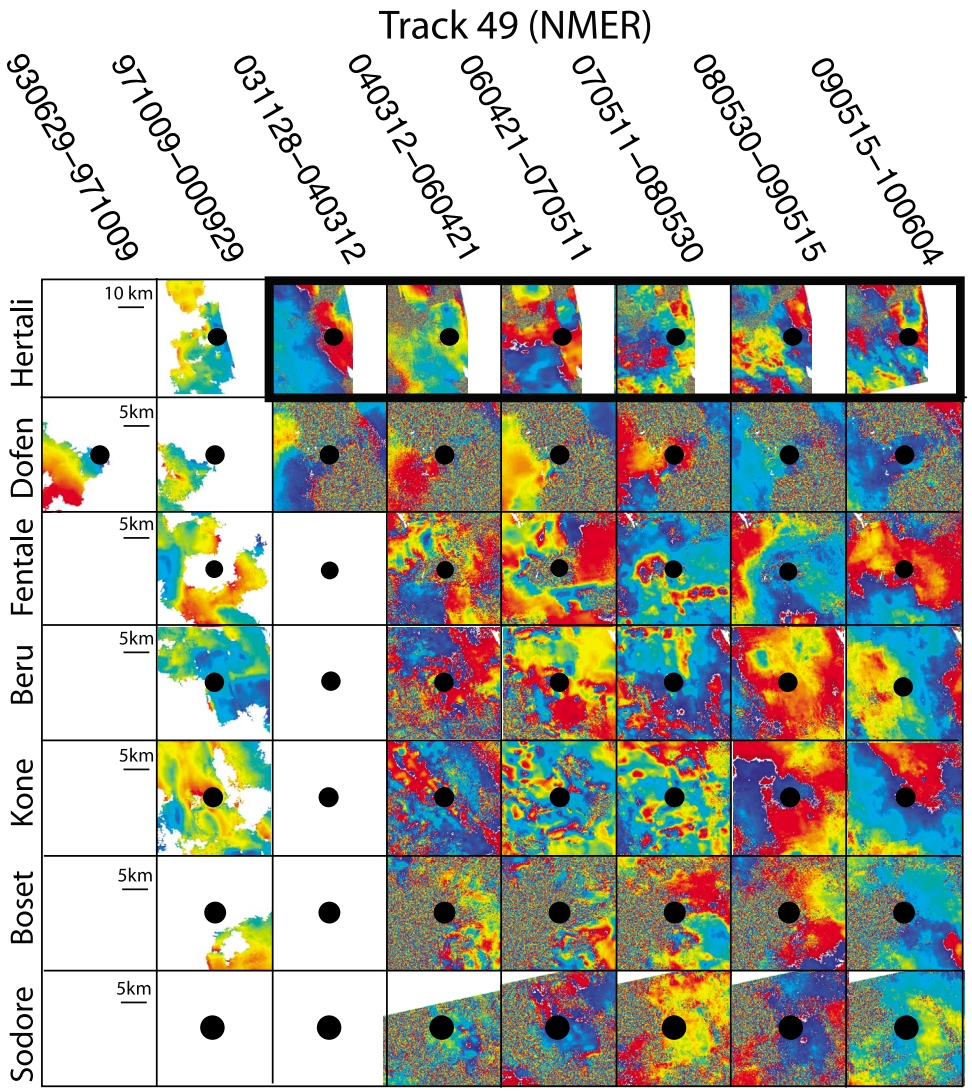

Figure 3. Survey interferograms from JERS, ERS, and Envisat for the northern MER. Each color cycle (fringe) represents 2.8 cm of displacement in the satellite line-of-sight. The black dot is the summit, according to the Smithsonian Database [*Siebert and Simkin*, 2002]. Black rectangles highlight interferograms in which deformation is visible.

[15] For each example, the same source geometry provides acceptable fits to both periods of uplift and subsidence and the variation in parameters between interferograms is significantly smaller than Monte Carlo error estimates (Table 1) based on realistic noise distributions [e.g., *Biggs et al.*, 2009b].

2.4. Temporal Characteristics

[16] The time series at Alutu shows two pulses of rapid inflation (10–15 cm) in 2004 and 2008 separated by a period of more gradual subsidence (Figure 6a). Periods of uplift began in 2008 and 2009 at Bora and Corbetti, respectively (Figures 6b and 6c). At Haledebi, the time series shows uplift

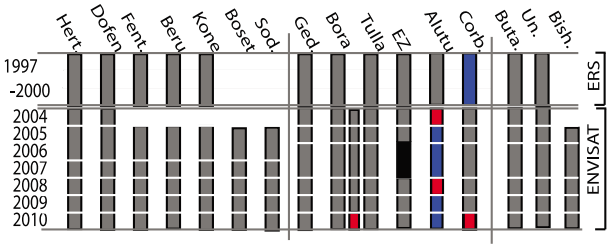

Figure 4. Chart showing the results of the ground deformation survey at each volcano. Red denotes uplift; blue denotes subsidence; grey denotes no deformation; black denotes no coherence; white denotes no interferogram available.

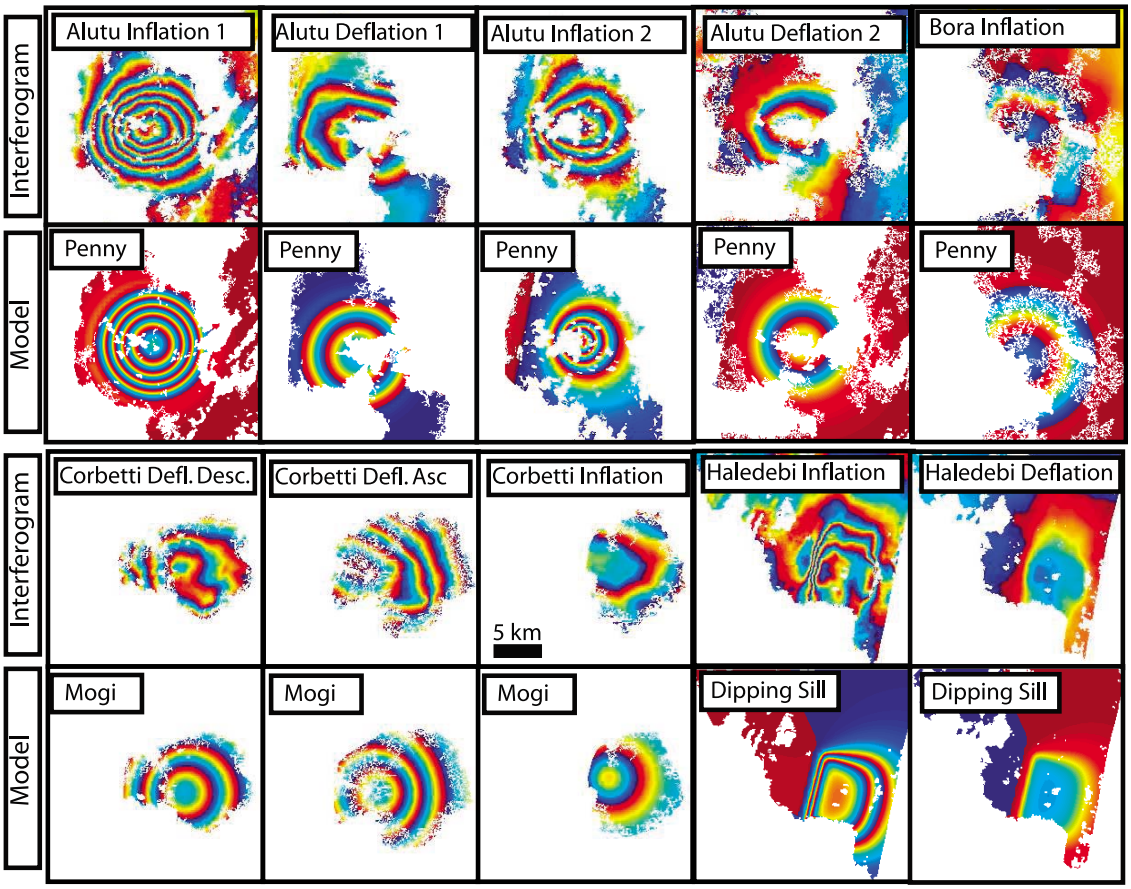

Figure 5. Example interferograms and models chosen to represent each period of significant displacement. Alutu inflation 1, 17 December 2003 to 18 August 2004; Alutu deflation 1, 22 September 2004 to 5 March 2008; Alutu inflation 2, 14 May 2008 to 1 December 2008; Alutu deflation 2, 14 January 2009 to 28 July 2010; Bora inflation, 26 December 2007 to 28 July 2010; Corbetti deflation (Desc), 23 September 1997 to 13 September 2000; Corbetti deflation (Asc), 28 September 1997 to 17 September 2000; Haledebi inflation, stacked rate for 8 interferograms between July 2007 and February 2008; Haledebi deflation, stacked rate for 122 interferograms between February 2008 and August 2010. Each fringe represents 2.8 cm of deformation. Model parameters are given in Table 1.

Table 1. Temporal and Spatial Characteristics of Observed Deformation[a]

	Start	Displacement (cm)	Length (days)	Decay (days)	Model	Depth (km)	Radius (km)
Alutu	Dec 2003	+15	260	230	Penny	0.7–2.5	2.8–8.9
	Sep 2004	−4.71	400	320	Penny	0.5–1.9	2.9–10
	Jul 2008	+9.9	150	230	Penny	0.7–2.4	4.0–8.2
	Dec 2008	<−4.3	>750	320	Penny		
Bora	Feb 2008	+5.3	900	1600	Penny	0.9–1.3	4.7–8.1
Corbetti	1994–1996[b]	>1.4	-	-	-	-	-
	1997–2000[b]	<14	-	-	Mogi	5.8–7.8	0
	-	−3.3	>2100	1500	-	-	-
	Aug 2009	+4.2	290	1700	Mogi	3.3–5.3	0
Haledebi	Jun 2007	+4.1	170	630	Sill	2.7–8.8	5.8 × 8
	Dec 2007	−5.4	>1000	6800	Sill	2.7–8.8	5.8 × 8

[a]All numbers are rounded to two significant figures. Errors in depth and radius reflect 1 sigma standard deviations from a log-Gaussian distribution.
[b]Dates refer to the period of the interferogram rather than the source process.

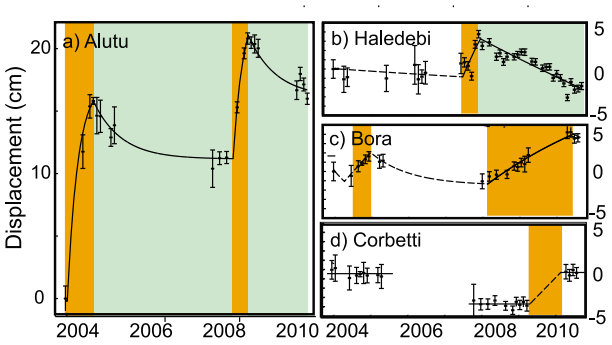

Figure 6. Time series of deformation from Envisat observations. (a) Alutu volcano showing two pulses of uplift in 2004 and 2008 with intervening phases of subsidence. (b) Haledebi showing uplift in 2007 followed by subsidence. (c) Bora-Berricio showing two pulses of uplift in 2004 and 2008–2010 with intervening subsidence. (d) Corbetti showing a pulse of uplift in 2009. Color blocks are used to indicate periods of uplift (orange) and subsidence (green) that are clearly above noise levels.

of ~4 cm from June to December 2007 followed by subsidence (Figure 6d).

[17] We paramaterize each period of deformation using an exponential function described by start date, magnitude and decay constant (Table 1). This approach provides a framework for comparison between edifices. Pulses of inflation at Alutu last <1 year (~9 and ~5 months) with longer periods of subsidence between (3.8 and >2.1 years). The decay constants are 7.5 months for inflation and 10.5 months for deflation. The magnitude of the inflation (10–15 cm) is larger than that of deflation (4–5 cm) producing a steplike pattern with overall inflation. The duration of uplift at Corbetti (~9 months) and Haledebi (~6 months) is similar to that at Alutu, but uplift at Bora occurred over a significantly longer period (~30 months). At Corbetti and Bora, inflation and deflation are more linear (i.e., the decay constant is >4 years). Although illustrated with an exponential fit, the time series at Haledebi shows systematic variations in rate, which are greater than the estimated errors.

3. Dynamics of Geothermal and Magmatic Systems

[18] Interpreting deformation patterns in terms of magma movement is often ambiguous since in many cases deformation does not culminate in eruption [e.g., *Biggs et al.*, 2009b], and conversely eruptions also occur without deformation [e.g., *Moran et al.*, 2006]. Although the structure of hydrothermal and magmatic systems in the Main Ethiopian Rift are poorly characterized, the depths inferred from our InSAR models (Table 1) are consistent with the boundary between the hydrothermal and magmatic systems for a generalized, conceptual model. Deformation alone is not sufficient to discriminate between magmatic and hydrothermal processes so we must rely on geological constraints on the expected characteristics of each system.

[19] Prior to a 7.3 MW pilot geothermal plant opening in the Alutu-Langano geothermal field in 1999, exploration drilling to 2.5 km encountered temperatures of 350°C. Extrusive products, including silicic tuffs, breccias, domes and obsidian flows, date from 155.8 ka to ~2000 ya [e.g., *Gianelli and Teklemariam*, 1993; *Gebregzabher*, 1986]. The rift-parallel faulting places structural controls on the small-scale, recent volcanic features (e.g., scoria cones) and on the geothermal system [*Gianelli and Teklemariam*, 1993; *Gizaw*, 1993]. Fluids upwell in a narrow, elongated zone along the fault, while inversion in the off-axis temperature structure indicates lateral outflow at shallower depths (<1 km) [*Gizaw*, 1993]. Disequilibria between alteration mineral assemblages, fluid inclusions and current well fluids [*Gianelli and Teklemariam*, 1993; *Valori et al.*, 1992] suggest the geothermal system is not in steady state and is episodically perturbed.

[20] The temporal pattern observed at Alutu, and to some extent, that at Bora and Corbetti, show remarkable similarities to that at Campi Flegrei, Italy where steady subsidence has been interrupted by pulses of uplift [*Chiodini et al.*, 2003]. This similarity is particularly surprising given the difference in tectonic setting and may suggest the volcanic processes responsible are independent of the regional stress regime. At Campi Flegrei, uplift may precede eruption (e.g., 7 m of uplift before 1538 Monte Nuovo eruption), but uplift alone does not necessarily imply an eruption will follow (~2 m of uplift was recorded in 1969–1972 and again in 1982–1984) [*Troise et al.*, 2007]. The ratios of horizontal to vertical deformation are significantly different during uplift and subsidence: uplift is attributed to a deep (~3 km) oblate source, and subsidence to a shallower prolate source. *Battaglia et al.* [2006] present a model in which the intrusion of magma takes place at the beginning of each period of unrest. Overpressure of magma or fluids of magmatic origin beneath an impermeable barrier cause uplift. When a major breach of this zone occurs brine and gases migrated to the brittle, lower

pressure, colder aquifer. Faulting and brecciation lead to efficient discharge of fluids by lateral migration resulting in subsidence.

[21] A similar concept may be applicable to Alutu: magma-driven uplift amplified by increased activity in the hydrothermal field, followed by subsidence associated with the hydrothermal field alone. However, a few crucial differences exist: (1) borehole evidence indicates that the fluid flow patterns of the geothermal reservoir are elongated parallel to the major structural control whereas the deformation patterns are near circular, and (2) unlike Campi Flegrei, the periods of uplift and subsidence can both be modeled by the same source. The shorter repeat times between pulses of uplift make Alutu an ideal candidate for multidisciplinary studies of these interactions, and future observations of this system may be key to understanding the processes at coupled magmatic-hydrothermal systems elsewhere.

4. Hazards and Resources in Continental Rifts

[22] Continental rifting involves several processes that represent a significant geohazard: dike intrusion, fault slip, silicic eruptions and ground cracking. Furthermore, many events demonstrate interactions between multiple processes [e.g., *Wright et al.*, 2006; *Ayele et al.*, 2009; *Biggs et al.*, 2009a; *Calais et al.*, 2008], thus magma migration beneath the silicic centers may have implications for the timing of dike intrusions, fault slip and ground cracking. In addition to the indicators of deep melt supply between Gedemsa and Dofen already discussed, we see signs of shallow magma storage further south between Corbetti and Bora. Although we only have detailed information for the past few decades in the MER, the repeat times of either intrusive and extrusive events are expected to be at least an order of magnitude longer than the archive of geodetic data (<20 years) presented here. Thus we acknowledge that our study may not be characteristic of the long-term behavior of the rift. Nonetheless we demonstrate that the area of significant geohazard extends south beyond Gedemsa.

[23] Ground cracks (open fissures) are typically observed following events such as earthquakes and dike intrusion, which involve significant deformation [*Asfaw*, 1982; *Rowland et al.*, 2007] and pose a significant hazard to infrastructure. We investigate possible links between cracks in Muleti village during anomalously heavy rainfall in 1996–1998 [*Ayalew et al.*, 2004] and Corbetti <20 km away. Unfortunately the cracks lie in a vegetated region that is incoherent in the 3 year interferogram that spans these events. Although Corbetti subsided by >14 cm of between 1997 and 2000, this is unlikely to have directly caused cracks of the observed size (up to 2.4 km by 2.5 m). However, *Clark* [1972] proposed a fissure development mechanism by which small-scale tectonic features are enlarged during heavy rainfall provided it occurs before the initial cracks are refilled by aeolian sand, slumping of the walls or sediment carried by light runoff [*Zellmer et al.*, 1985]. Applied to our observations, this implies that the underlying deformation was continuous during 1996–1998, producing small-scale cracks above which fissures formed in the soil during heavy rainfall. Recent uplift at Corbetti following a 10 year hiatus in both deformation and cracking, may echo the uplift observed between 1994 and 1996 and could herald another period of cracking and resulting disruption to infrastructure.

[24] Ethiopia, like Iceland, has high geothermal potential: rifting above anomalously hot mantle promotes the emplacement of magma into the shallow crust. By detecting shallow magma storage driving hydrothermal circulation in locations such as Alutu we demonstrate the potential of InSAR as a prospecting tool for the geothermal industry. Previous exploration has mirrored the belief that peak melt supply, geohazard and geothermal potential lie between Gedemsa and Dofen (Figure 1). Our observations confirm that the Alutu-Langano power plant is located above the most active zone of magma migration in the MER and identify additional locations that warrant more detailed exploration (e.g., Corbetti, Bora).

5. Global Volcanism and Continental Deformation

[25] Observations of shallow magma storage beneath central volcanoes in the MER complement those from Kenyan Rift [*Biggs et al.*, 2009b], the Afar Depression [*Wright et al.*, 2006; *Grandin et al.*, 2009; *Keir et al.*, 2011], the Virunga volcanoes [*Wauthier et al.*, 2010] and Tanzania [*Calais et al.*, 2008; *Biggs et al.*, 2009a; *Baer et al.*, 2008]. Together, these studies demonstrate that ~yearlong inflation of shallow magma-plumbing systems is a common characteristic of continental rifts. Of the four observed deformation signals, two are directly associated with well-known volcanic edifices (Alutu and Corbetti) and a third is located within an active area close to other volcanoes (Bora). However, unlike observations from the Afar and Tanzania, where

Table 2. Comparison Between Volcano Records for Different Tectonic Settings[a]

	Total	Historical	Deformation	Ratio
E. Africa	110	20	14	8:1.4:1
Iceland	30	17	8	4:2.1:1
Aleutians	91	42	15	6:2.8:1
Andes	175	62	18	10:3.4:1
Overall	406	141	55	7:2.5:1

[a]The total number of volcanoes and the number of these with historical eruptions are taken from the Smithsonian catalog. The number of volcanoes with deformation signals is taken from *Fournier et al.* [2010] and updated using this study.

dike intrusion clearly accommodates a significant component of the divergent plate motion [*Wright et al.*, 2006; *Grandin et al.*, 2009; *Calais et al.*, 2008; *Baer et al.*, 2008; *Biggs et al.*, 2009a; *Keir et al.*, 2011], the InSAR observations presented here do not directly constrain the contribution of shallow magmatism to extension.

[26] Compilations of magma fluxes show little variation between tectonic settings [*White et al.*, 2006], yet there are differences in volcano deformation between arcs [*Fournier et al.*, 2010]. We use the updated record of volcano deformation, now 14 in East Africa, to compare a typical ocean-ocean arc (Aleutians), a continental arc (Andes), an oceanic hot spot (Iceland) and a continental rift (E. Africa). Table 2 gives a comparison of three measures of regional volcanic activity: (1) the total number of volcanoes [*Siebert and Simkin*, 2002]; (2) the number of volcanoes with historical eruptions [*Siebert and Simkin*, 2002], and (3) the number of volcanoes with known deformation signatures. The proportion of deforming volcanoes varies from 4:1 in Iceland to 10:1 in the Andes and the updated value for East Africa of 8:1 lies within this range. However, the ratio of volcanoes with historical eruptions ranges from 2.1 in Iceland to 3.4 in the Andes, but is only 1.4 in East Africa. Since the proportion of historically active volcanoes is much lower in East Africa than in other locations, we attribute this difference to a reporting bias for historical eruptions: the written record is shorter, and fewer deposits have eruption dates. Thus following this study, the number of volcanoes with recorded deformation signatures for volcanoes in East Africa is comparable to other regions and we see no systematic variation between tectonic settings.

6. Conclusions

[27] We have demonstrated that pulses of deformation have occurred at four volcanic edifices in the MER (Alutu, Corbetti, Bora and Haledebi) between 1993 and 2010. This raises the number of volcanoes known to be deforming in East Africa to 14, comparable to many arcs despite the smaller number of recorded eruptions. Our observations indicate a shallow (<10 km), frequently replenished zone of magma storage associated with volcanic edifices and add to the growing body of observations that indicate shallow magmatic processes operating on a decadal timescale are common throughout the East African Rift. In the absence of detailed historical records of volcanic activity, satellite-based observations of monitoring parameters, such as deformation, could play an important role in assessing volcanic hazard.

Acknowledgments

[28] JB was funded by the European Space Agency Changing Earth Science Network, COMET+, and NERC New Investigator grant NE/I001816/1; IB was funded by the Leverhulme Trust; DK was funded by NERC. We thank G. Demisee, J. Gottsman, J. M. Kendall, and D. Pyle for useful discussions and the Editor Thorsten Becker, Cindy Ebinger, and one anonymous reviewer for their helpful comments. We thank ESA for access to their archive of ERS and Envisat images.

References

Abebe, B., V. Acocella, T. Korme, and D. Ayalew (2007), Quaternary faulting and volcanism in the Main Ethiopian Rift, *J. Afri. Earth Sci.*, *48*(2–3), 115–124, doi:10.1016/j.jafrearsci.2006.10.005.

Asfaw, L. (1982), Development of earthquake-induced fissures in the Main Ethiopian Rift, *Nature*, *297*, 393–395.

Aspinall, W., M. Auker, T. Hincks, S. Mahony, F. Nadim, J. Pooley, S. Sparks, and E. Syre (2011), Volcano hazard and exposure in GFDRR priority countries and risk mitigation measures, *Volcano Risk Study 0100806-00-1-R*, Global Facil. for Disaster Reduct. and Recovery, Washington, D. C.

Ayalew, L., H. Yamagishi, and G. Reik (2004), Ground cracks in Ethiopian rift valley: Facts and uncertainties, *Eng. Geol.*, *75*, 309–324.

Ayele, A., D. Keir, C. Ebinger, T. Wright, G. Stuart, W. Buck, E. Jacques, G. Ogubazghi, and J. Sholan (2009), September 2005 mega-dike emplacement in the Manda-Harraro nascent oceanic rift (Afar depression), *Geophys. Res. Lett.*, *36*, L20306, doi:10.1029/2009GL039605.

Baer, G., Y. Hamiel, G. Shamir, and R. Nof (2008), Evolution of a magma-driven earthquake swarm and triggering of the nearby Oldoinyo Lengai eruption, as resolved by InSAR, ground observations and elastic modeling, East African Rift, 2007, *Earth Planet. Sci. Lett.*, *272*, 339–352.

Bastow, I., S. Pilidou, J.-M. Kendall, and G. Stuart (2010), Melt-induced seismic anisotropy and magma assisted rifting in Ethiopia: Evidence from surface waves, *Geochem. Geophys. Geosyst.*, *11*, Q0AB05, doi:10.1029/2010GC003036.

Bastow, I., D. Keir, and E. Daly (2011), The Ethiopia Afar Geoscientific Lithospheric Experiment (EAGLE): Probing

the transition from continental rifting to incipient seafloor spreading, in *Volcanism and Evolution of the African Lithosphere*, edited by L. Beccaluva, G. Bianchini, and M. Wilson, *Spec. Pap. Geol. Soc. Am.*, *478*, 1–26, doi:10.1130/2011.2478(04).

Battaglia, M., C. Troise, F. Obrizzo, F. Pingue, and G. De Natale (2006), Evidence for fluid migration as the source of deformation at Campi Flegrei caldera (Italy), *Geophys. Res. Lett.*, *33*, L01307, doi:10.1029/2005GL024904.

Berardino, P., G. Fornaro, R. Lanari, and E. Sansosti (2002), A new algorithm for surface deformation monitoring based on small baseline differential SAR Interferograms, *IEEE Trans. Geosci. Remote Sens.*, *40*, 2375–2383.

Biggs, J., F. Amelung, N. Gourmelen, T. H. Dixon, and S. Kim (2009a), InSAR observations of 2007 Tanzania rifting episode reveal mixed fault and dyke extension in an immature continental rift, *Geophys. J. Int.*, *179*, 549–558, doi:10.1111/j.1365-246X.2009.04262.x.

Biggs, J., E. Anthony, and C. Ebinger (2009b), Multiple inflation and deflation events at Kenyan volcanoes, East African Rift, *Geology*, *37*, 979–982, doi:10.1130/G30133A.1.

Biggs, J., Z. Lu, T. Fournier, and J. T. Freymueller (2010), Magma flux at Okmok Volcano, Alaska, from a joint inversion of continuous GPS, campaign GPS, and interferometric synthetic aperture radar, *J. Geophys. Res.*, *115*, B12401, doi:10.1029/2010JB007577.

Calais, E., et al. (2008), Strain accommodation by slow slip and dyking in a youthful continental rift, East Africa, *Nature*, *456*, 783–787, doi:10.1038/nature07478.

Chiodini, G., M. Todesco, S. Caliro, C. Del Gaudio, G. Macedonio, and M. Russo (2003), Magma degassing as a trigger of bradyseismic events: The case of Phlegrean Fields (Italy), *Geophys. Res. Lett.*, *30*(8), 1434, doi:10.1029/2002GL016790.

Clark, M. (1972), Surface rupture along the Coyote Creek fault, the Borrego Mountain earthquake of April 9, 1968, *U.S. Geol. Surv. Prof. Pap.*, *787*, 55–86.

Ebinger, C. J., and M. Casey (2001), Continental breakup in magmatic provinces: An Ethiopian example, *Geology*, *29*, 527–530.

Ebinger, C. J., and N. J. Hayward (1996), Soft plates and hot spots: Views from Afar, *J. Geophys. Res.*, *101*, 21,859–21,876, doi:10.1029/96JB02118.

Ebinger, C. T., D. Harding, S. Tesfaye, S. Kelley, and D. Rex (2000), Rift deflection, migration, and propagation: Linkage of the Ethiopian and Eastern rifts, Africa, *Geol. Soc. Am. Bull.*, *112*, 163–176.

Fialko, Y., M. Simons, and D. Agnew (2001), The complete (3-D) surface displacement field in the epicentral area of the 1999 M_w7.1 Hector Mine earthquake, California, from space geodetic observations, *Geophys. Res. Lett.*, *28*(16), 3063–3066.

Fournier, T. J., M. Pritchard, and S. Riddick (2010), Duration, magnitude, and frequency of subaerial volcano deformation events: New results from Latin America using InSAR and a global synthesis, *Geochem. Geophys. Geosyst.*, *11*, Q01003, doi:10.1029/2009GC002558.

Gebregzabher, Z. (1986), Hydrothermal alteration minerals in Aluto Langano geothermal wells, Ethiopia, *Geothermics*, *15*(5–6), 735–740, doi:10.1016/0375-6505(86)90086-6.

Gianelli, G., and M. Teklemariam (1993), Water-rock interaction processes in the Aluto-Langano geothermal field (Ethiopia), *J. Volcanol. Geotherm. Res.*, *56*, 429–445, doi:10.1016/0377-0273(93)90007-E.

Gizaw, B. (1993), Aluto-Langano geothermal field, Ethiopian rift valley: physical characteristics and the effects of gas on well performance, *Geothermics*, *22*(2), 101–116, doi:10.1016/0375-6505(93)90050-W.

Grandin, R., et al. (2009), September 2005 Manda Hararo-Dabbahu rifting event, Afar (Ethiopia): Constraints provided by geodetic data, *J. Geophys. Res.*, *114*, B08404, doi:10.1029/2008JB005843.

Keir, D., I. Bastow, K. Whaler, C. Dg, and S. Hautot (2009), Lower crustal earthquakes near the ethiopian rift induced by magmatic processes, *Geochem. Geophys. Geosyst.*, *10*, Q0AB02, doi:10.1029/2009GC002382.

Keir, D., C. Pagli, I. D. Bastow, and A. Ayele (2011), The magma-assisted removal of Arabia in Afar: Evidence from dike injection in the Ethiopian rift captured using InSAR and seismicity, *Tectonics*, *30*, TC2008, doi:10.1029/2010TC002785.

Kendall, J.-M., S. Pilidou, D. Keir, I. Bastow, G. Stuart, and A. Ayele (2006), Mantle upwellings, melt migration and the rifting of Africa: Insights from seismic anisotropy, in *The Afar Volcanic Province Within the East African Rift System*, edited by G. Yirgu, C. J. Ebinger, and P. K. H. Maguire, *Geol. Soc. Spec. Pub.*, *259*, 271–293.

Keranen, K., S. Klemperer, and R. Gloaguen (2004), Three-dimensional seismic imaging of a protoridge axis in the Main Ethiopian rift, *Geology*, *32*, 949–952, doi:10.1130/G20737.1.

Mackenzie, G., H. Thybo, and P. Maguire (2005), Crustal velocity structure across the Main Ethiopian Rift: results from two-dimensional wide-angle seismic modelling, *Geophys. J. Int.*, *162*, 994–1006.

Maguire, P., et al. (2006), Crustal structure of the northern main ethiopian rift from the eagle controlled-source survey; a snapshot of incipient lithospheric break-up, in *The Afar Volcanic Province Within the East African Rift System*, edited by G. Yirgu, C. J. Ebinger, and P. K. H. Maguire, *Geol. Soc. Spec. Pub.*, *259*, 269–292.

Massonnet, D., M. Rossi, C. Carmona, F. Adragna, G. Peltzer, K. Fiegl, and T. Rabaute (1993), The displacement field of the Landers Earthquake mapped by radar interferometry, *Nature*, *364*, 138–142.

Mazzarini, F., and I. Isola (2010), Monogenetic vent self-similar clustering in extending continental crust: Examples from the East African Rift system, *Geosphere*, *6*, 567–582.

Mogi, K. (1958), Relations between eruptions of various volcanoes and the deformations of the ground surfaces around them, *Bull. Earthquake Res. Inst.*, *36*, 99–134.

Moran, S. C., O. Kwoun, T. Masterlark, and Z. Lu (2006), On the absence of InSAR-detected volcano deformation spanning the 1995, 1996 and 1999 eruptions of Shishaldin Volcano, Alaska, *J. Volcanol. Geotherm. Res.*, *150*, 119–131, doi:10.1016/j.jvolgeores.2005.07.013.

Okada, Y. (1985), Surface deformation due to shear and tensile faults in a half-space, *Bull. Seismol. Soc. Am.*, *75*, 1135–1154.

Pritchard, M. E., and M. Simons (2004), An InSAR-based survey of volcanic deformation in the central Andes, *Geochem. Geophys. Geosyst.*, *5*, Q02002, doi:10.1029/2003GC000610.

Rampey, M. L., C. Oppenheimer, D. M. Pyle, and G. Yirgu (2010), Caldera-forming eruptions of the Quaternary Kone Volcanic Complex, Ethiopia, *J. Afri. Earth Sci.*, *58*, 51–66, doi:10.1016/j.jafrearsci.2010.01.008.

Rooney, T., I. Bastow, and D. Keir (2011), Insights into extensional processes during magma assisted rifting: Evidence

from aligned scoria cones, *J. Volcanol. Geotherm. Res.*, *201*, 83–96, doi:10.1016/j.jvolgeores.2010.07.019.

Rowland, J. V., E. Baker, C. J. Ebinger, D. Keir, T. Kidane, J. Biggs, N. Hayward, and T. J. Wright (2007), Fault growth at a nascent slow-spreading ridge: 2005 Dabbahu rifting episode, *Afar*, *171*, 1226–1246, doi:10.1111/j.1365-246X.2007.03584.x.

Siebert, L., and T. Simkin (2002), Volcanoes of the World: An Illustrated Catalog of Holocene Volcanoes and Their Eruptions, *Global Volcanism Program Digital Inf. Ser.*, *GVP-3*, Smithsonian Inst., Washington, D. C. [Available at http://www.volcano.si.edu/world/.]

Tiberi, C., C. Ebinger, V. Ballu, G. Stuart, and B. Oluma (2005), Inverse models of gravity data from the Red Sea-Aden-East African rifts triple junction zone, *Geophys. J. Int.*, *163*, 775–787, doi:10.1111/j.1365-246X.2005.02736.x.

Troise, C., G. De Natale, F. Pingue, F. Obrizzo, P. De Martino, U. Tammaro, and E. Boschi (2007), Renewed ground uplift at Campi Flegrei caldera (Italy): New insight on magmatic processes and forecast, *Geophys. Res. Lett.*, *34*, L03301, doi:10.1029/2006GL028545.

Valori, A., M. Teklemariam, and G. Gianelli (1992), Evidence of temperature increase of CO_2-bearing fluids from Aluto-Langano geothermal field (Ethiopia): A fluid inclusions study of deep wells LA-3 and LA-6, *Eur. J. Mineral*, *4*(5), 907–919.

Wauthier, C., V. Cayol, A. Hooper, F. Kervyn, P. Marinkovic, N. D'Oreye, and M. P. Poland (2010), Activity of Nyiragongo and Nyamulagira Volcanoes (Dem. Rep. of Congo) Revealed Using Geological, Geophysical and InSAR data, Abstract G21D-05 presented at 2010 Fall Meeting, AGU, San Francisco, Calif., 13–17 Dec.

White, S. M., J. A. Crisp, and F. J. Spera (2006), Long-term volumetric eruption rates and magma budgets, *Geochem. Geophys. Geosyst.*, *7*, Q03010, doi:10.1029/2005GC001002.

Woldegabriel, G., J. Aronson, and R. Walter (1990), Geology, geochronology, and rift basin development in the central sector of the Main Ethiopia Rift, *Geol. Soc. Am. Bull.*, *102*, 439–458.

Wolfenden, E., C. Ebinger, G. Yirgu, A. Deino, and D. Ayalew (2004), Evolution of the northern Main Ethiopian Rift: birth of a triple junction, *Earth Planet. Sci. Lett.*, *224*, 213–228.

Wright, T., C. Ebinger, J. Biggs, A. Ayele, G. Yirgu, D. Keir, and A. Stork (2006), Magma-maintained rift segmentation at continental rupture in the 2005 Afar dyking episode, *Nature*, *442*, 291–294, 2006.

Zellmer, J. T., G. Roquemore, and B. Blackerby (1985), Modern tectonic cracking near the Garlock Fault, California, *Geol. Soc. Am. Bull.*, *96*, 1037–1042.